Materials Science and Engineering A 384 (2004) 151–161

www.elsevier.com/locate/msea

Failure mechanisms of dense vertically-cracked thermal barrier coatings

Manish Madhwal [a], Eric H. Jordan [b,*], Maurice Gell [a]

[a] *Department of Metallurgy and Materials Engineering, Institute of Materials Science, School of Engineering, University of Connecticut, Storrs, CT 06269, USA*

[b] *Department of Mechanical Engineering, University of Connecticut, Storrs, CT 06269, USA*

Received 20 October 2003; received in revised form 24 May 2004

Abstract

Failure lives and failure mechanisms of samples coated with dense vertically-cracked (DVC) thermal barrier coatings (TBCs) were studied in cyclic furnace tests using 1-h cycles at three different temperatures: 1100 °C, 1121 °C and 1151 °C. Average failure life at 1100 °C cycles was six times longer than at 1151 °C. At all the three temperatures in the 1-h cycle tests, progressive cracking of the TBC near and parallel to the interface with the bond coat was observed beginning typically at 25% of the expected failure life. The measured density of such cracks increased almost linearly with cycles. Strains imposed on the TBC by progressive distortion of the bond coat (rumpling) are believed to be primarily responsible for the observed cracking with a secondary role played by the formation of chromia in the bond coat.

Keywords: Dense; Cracked; Thermal barrier coatings; Spallation; Rumpling

1. Introduction

Thermal barrier coatings (TBCs) are used to protect and insulate hot-section metal components in gas turbine engines (propulsion and power generation) [1–5]. TBCs lower the temperature at the metal surface, thus improving component durability. The dense vertically-cracked (DVC) plasma-sprayed TBC used in this study, like most TBC systems, consists of four layers: (1) a Ni-based superalloy substrate (GTD-111), (2) an oxidation-resistant metallic NiCrAlY bond coat, (3) thermally-grown oxide (TGO) typically α-alumina, formed during heat treatment or in service due to oxidation of the bond coat and (4) a ceramic top coat 7–8 wt.% yittria-stabilised zirconia (YSZ) deposited by air plasma spray (APS). The durability of a TBC system depends on a combination and interaction of several phenomena in these four mentioned layers [5–8], for example: (i) thermal expansion mismatch between the TGO and bond coat, (ii) formation of TGO between the bond coat and the TBC, (iii) Al depletion in the bond coat, (iv) bond coat rumpling, (v) degradation of the bond coat strength with cycling and (vi) crack initiation growth and link up. The specific combination of failure mechanisms depends on factors such as cycle duration, initial bond coat roughness and chemistry and test temperature. The present paper deals with the detailed behavior of a specific TBC and test conditions, other failure behaviors can and have been observed in other systems.

Plasma-sprayed coatings are prone to large scale spallation as the cracks induced due to thermal stresses propagate to failure. Vertical microcracks (see Fig. 1) are deliberately introduced in the ceramic top coat of the coating test in the present case to relieve thermal mismatch stresses, thus reducing tendency of the ceramic to crack and buckle [9]. In the plasma spray process, the molten YSZ particle forms splats on impacting the substrate surface, the coating is deposited layer by layer on the substrate and superimposing the splats within each layer. Each layer upon solidification forms vertical cracks due to shrinkage. The cracks in adjacent layers connect to form through coating thickness cracks.

In this study, commercially produced DVC coatings were thermally cycled to various fractions of their failure lives and then characterized. Three different cycling temperatures were used to determine the failure lives of the coatings and their respective spallation mechanisms.

* Corresponding author. Tel.: +1 860 486 2371; fax: +1 860 486 5088.
E-mail address: jordan@engr.uconn.edu (E.H. Jordan).

0921-5093/$ – see front matter © 2004 Elsevier B.V. All rights reserved.
doi:10.1016/j.msea.2004.05.061

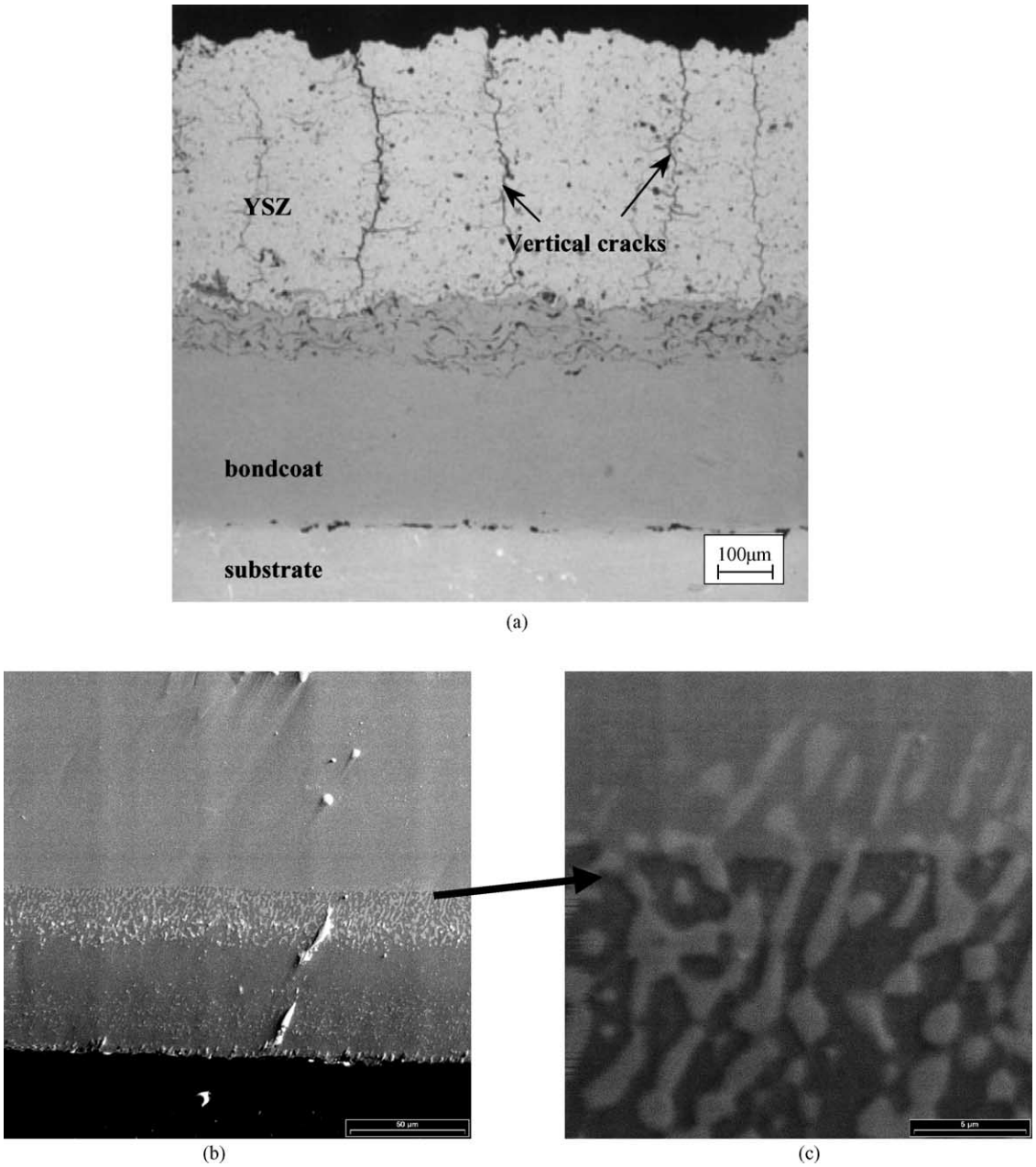

Fig. 1. (a) Cross-sectional SEM micrograph showing various layers in the TBC, (b) cross-sectional micrograph of the specimen bottom surface and (c) magnified image of the two-phase region of the NiCrAlY bond coat.

2. Experimental procedure

2.1. TBC specimens

The dense vertically-cracked plasma-sprayed coatings used in this study were supplied by a commercial coating manufacturer. All specimens were disk shaped (25.4 mm diameter, 3.2 mm thick) with a superalloy substrate (GTD-111), an air plasma-sprayed bond coat (NiCrAlY, ∼250 μm thick) with an air plasma-sprayed ceramic top coat (8% YSZ, ∼300 μm thick) (Table 1). A 100 μm thick bond coat was also deposited on the bottom of these coatings (see Fig. 1), so that oxidation of bare and buried bond coats could be studied.

2.2. Thermal cycling

A bottom-loading programmable cyclic furnace was used for determining cyclic lives. Each 1-h cycle consisted of a rapid (10 min) heating to a specified temperature (1100 °C, 1121 °C and 1151 °C), a hold of 40 min followed by a 10 min cool down to near-room temperature. The failure criterion was defined as ∼50% buckling or spallation of the ceramic top coat. Specimens were removed at different fractions of

Table 1
Typical composition of the different layers in the DVC TBC system used in this study

TBC system layer	Material	Composition (wt.%)
Substrate	GTD-111 polycrystalline superalloy	13.5 Cr, 9.5 Co, 4.75 Ti, 3.8 W, 3.3 Al, 2.7 Ta, 1.53 Mo, 0.23 Fe, 0.09 C, 0.01 B, Bal. Ni
Bond coat	APS NiCrAlY	22 Cr, 10 Al, 1 Y, Bal. Ni
Ceramic top coat	APS YSZ	8 Y_2O_3 in ZrO_2

their life for cross-sectional studies, while others were observed for signs of failure and were cycled until the failure criterion was met.

2.3. Metallography

TBC specimens were sectioned at various life fractions using a low-speed diamond saw. Specimens were mounted in a low-viscosity resin and vacuum impregnated to preserve the cross-sectional and edge features. Samples with greater than 20 1-h cycles were vacuum mounted before sectioning to avoid artifacts due to cutting and polishing. The mounted samples were then ground using silicon carbide papers and polished to a 1-μm surface finish using 3 μm and 1 μm diamond paste. Final polishing with 0.05 γ-alumina was performed to reveal sub-micron details. The samples were then cleaned using routine metallographic procedures. The sample cross-sections, top and bottom surfaces were observed using environmental scanning electron microscope (ESEM 2020, Philips) and conventional scanning electron microscope (Amray 1000). Elemental mapping was done using an energy dispersive spectrometer (EDAX 9100).

2.4. Image analysis

Bond coat roughness (rumpling) measurements were conducted across the entire cross-sections of the TBC samples at various fractions of their life at 1121 °C using image analysis. SEM micrographs at optimal magnification (to extract relevant and statistically correct results) were taken, maintaining continuity between images across the entire visible cross-sections, and Microgop 2000 image analysis software was used to measure rumpling. Internal oxidation of the bond coat poses problems for automatic recognition in image analysis software, as gray contrast for TGO and internal oxides are similar. To overcome this problem, the TGO–bond coat interface was manually drawn in each micrograph and then processed using image analysis software for rumpling measurements. Average roughness (R_a) measurements were calculated as (1):

$$R_a = \frac{(\sum_{i=1}^{m} P_i - \sum_{i=1}^{m} V_i)}{m} \quad (1)$$

where P_i and V_i are the peak and valley heights, respectively, of m peaks and m valleys. A sampling length of 15 mm was used for each sample.

3. Experimental results

3.1. Failure lives

The average failure lives at 1100 °C, 1121 °C and 1151 °C are given in Fig. 2. The average spallation life is nearly halved when the cycling temperature is increased from 1100 °C to 1121 °C. A difference of 51 °C in the temperature at the hot time resulted in six times decrease in the failure life. The samples showed consistent spallation lives with small scatter at a particular temperature. However, the spallation lives showed a strong dependence on temperature. Contrary to reported service experience, the failure lives of these DVC TBCs are somewhat lower than those of good APS coatings tested in the same furnace. It will be shown that the rate of bond coat oxidation and rumpling may account for these surprising results.

3.2. SEM observations

Fig. 3 shows the typical as-received microstructure of the dense vertically-cracked APS TBC near the ceramic–bond coat interface. There are oxides within the bond coat (A) prior to thermal cycling and a thin discontinuous oxide layer along the interface (B). The presence of oxides in the as-received specimen is typical of the APS bond coat. Intersplat porosities and splat boundaries can also be seen in the ceramic top coat typical to the APS process. The specimens when cycled to failure always fail with the whole ceramic layer spalling as one piece from the substrate (Fig. 4). Once the failure life has been determined, the SEM cross-sections

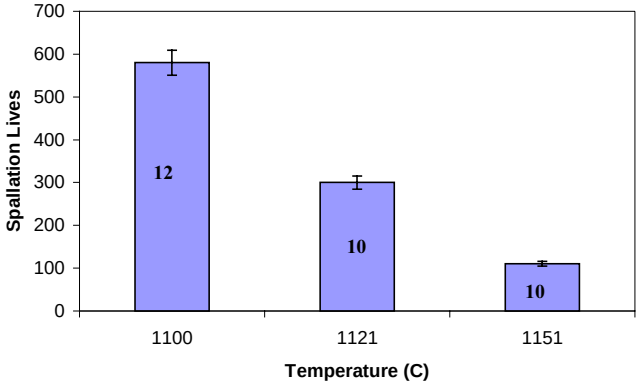

Fig. 2. Total cycles to failure for 1100 °C, 1121 °C and 1151 °C for DVC TBC system. The number on the bar represents number of samples tested.

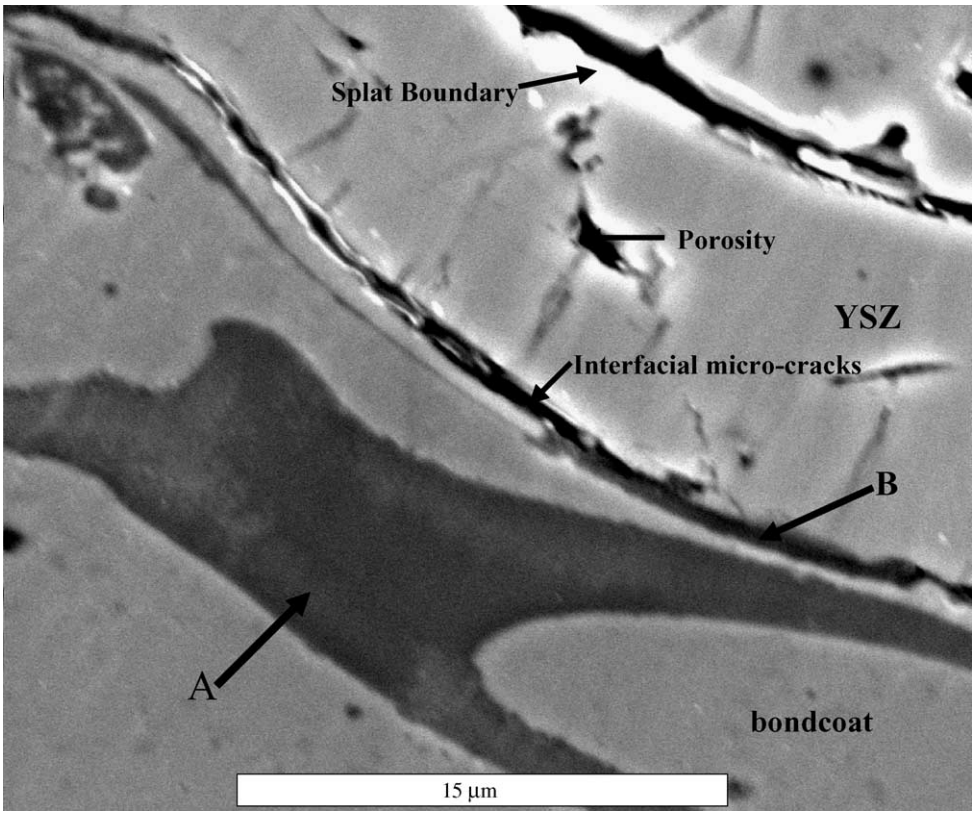

Fig. 3. Typical as-received DVC TBC cross-section at the interface showing characteristics of the ceramic top coat and bond coat.

at different life fractions reveal further details concerning the crack initiation, propagation and linkage in this coating (Fig. 5). The discontinuous oxide layer in the as-received cross-sections becomes uniform and starts growing with increasing cycles. The oxides in the bond coat seen in the as-received cross-section grow progressively due to considerable oxidation of the bond coat. These oxides within the bond coat are a result of pores connected to interfaces that provide pathway for oxygen ingress [10]. No obvious signs of significant sintering appears in any micrographs. Extensive sintering would be expected at higher temperatures [11].

Cracks in the ceramic start appearing as soon as 25% of the failure life with lengths as much as 150–200 μm and maximum crack opening displacements of 10–15 μm. The cracks due to thermal cycling are easily distinguishable from other microcracks in the as-received coating. The crack locations and propagation path are essentially independent of the pre-existing vertical cracks. The association of transverse

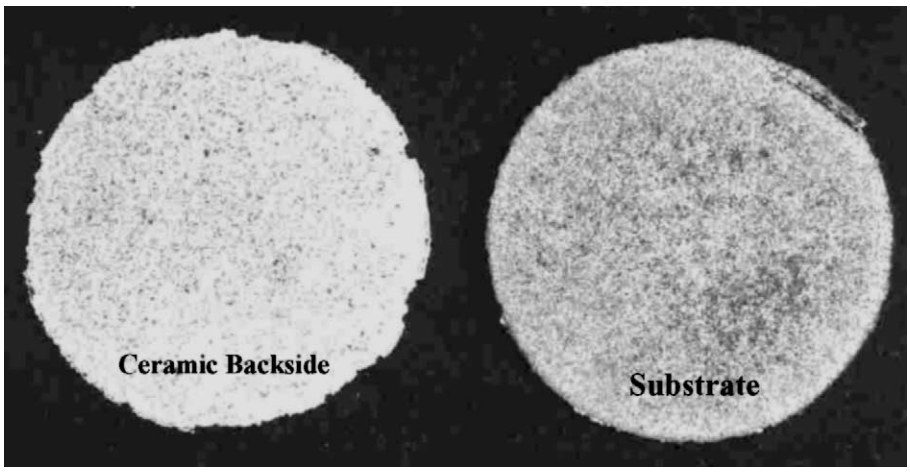

Fig. 4. Macro photographs of the failed sample showing the top view of the spalled substrate and the underside of the spalled ceramic.

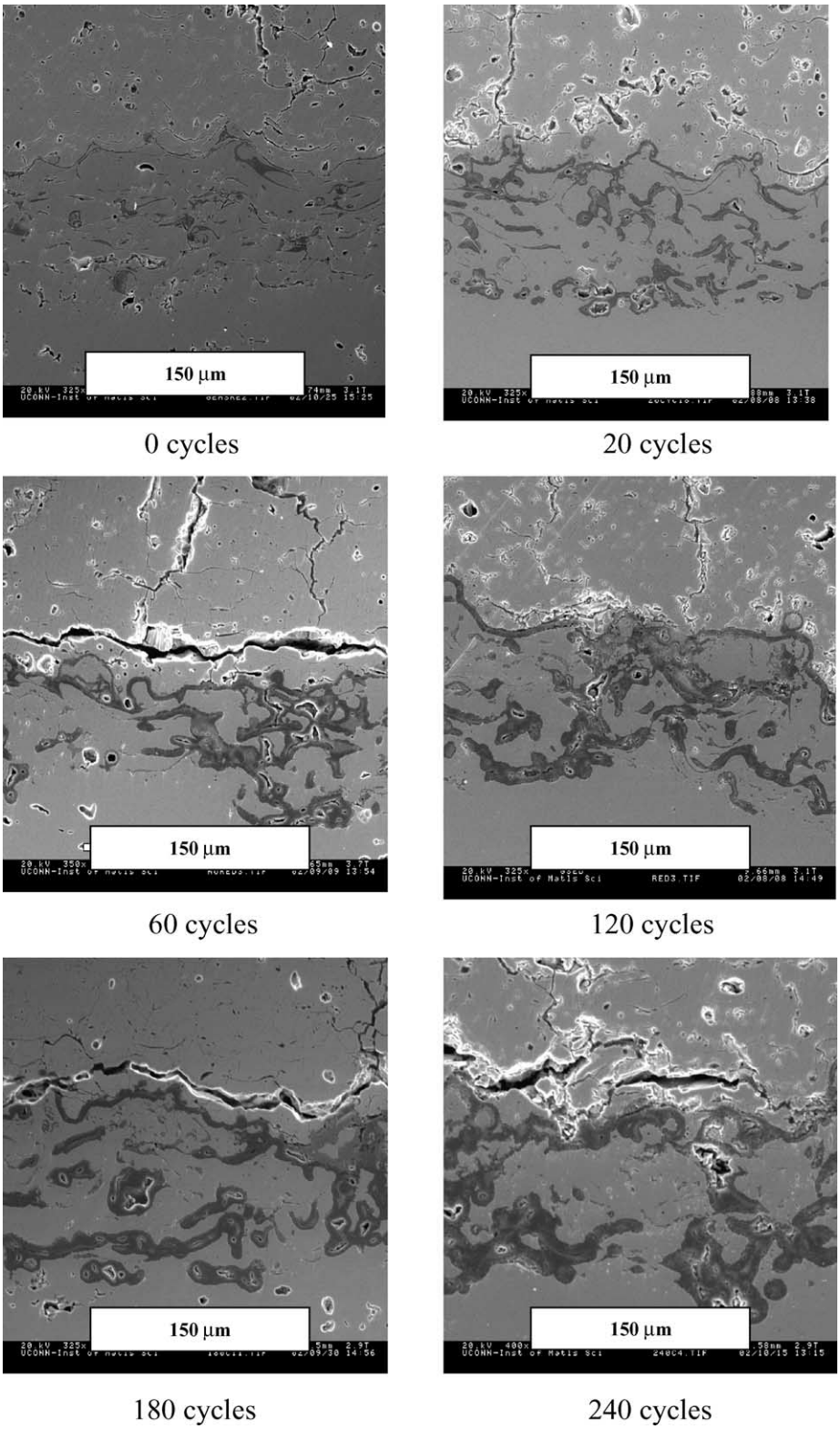

Fig. 5. Cross-section SEM micrographs of the samples at various fractions of cyclic life at 1121 °C showing the crack propagation in the ceramic.

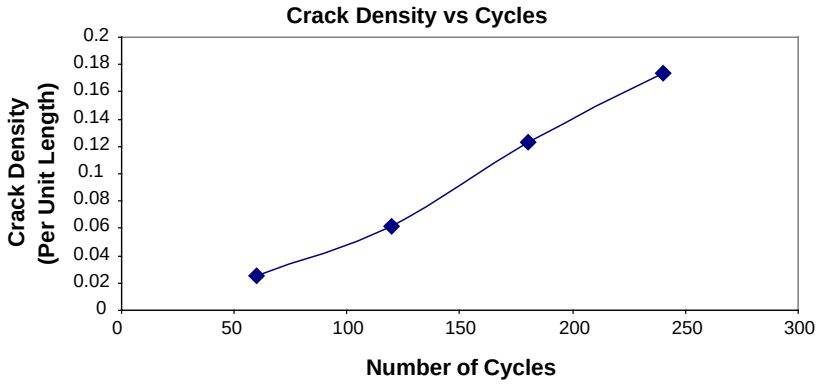

Fig. 6. Crack density measured across the entire specimen cross-section plotted against number of thermal cycles (1121 °C).

interface cracks with vertical cracks has been shown for thermal shock loading [12], but does not occur for this experiment where the temperature gradient is essentially zero. In the present case there is no cracking at the interface. The characteristics of the cracks due to cycling are as follows:

1. Cracks due to thermal cycling appear parallel to the TGO–ceramic interface.
2. Crack opening displacements are quite large as compared to intersplat boundaries
3. They are entirely in the ceramic, usually within a 50 μm of the ceramic–TGO interface.

The cross-section micrographs of the samples with increasing thermal cycles (Fig. 5) show the propagation of the cracks in the ceramic with cycles. The cracks increase in length with progressive cycles, and their eventual linkage leads to the spallation of the TBC entirely in the ceramic. The crack density of such cracks measured across the entire cross-section of the samples at various fractions of their spallation life is shown in Fig. 6. Crack density is recorded as crack length per unit length of the interface. At any one interface location, there is at most one crack between the interface and the free surface of the TBC. This measure of crack density under the assumption that the section is random corresponds the area fraction in plan view, lost due to cracking. The crack density was found to vary linearly with thermal cycling. Extrapolation of the crack density to final failure leads to crack densities of ≈0.2 suggesting that unstable cracking occurs around this damage level. Cross-section micrographs of the failed samples (Fig. 7a) further show that the cracking was entirely in the ceramic, the cross-section of the failed substrate shows that the failure occurred well above the TGO–ceramic interface, thus leaving behind ceramic on the substrate. When the failed ceramic top coat cross-section is studied, we see no remnant TGO attached to the ceramic. However, there are occasional exceptions where the cracks in the ceramic top coat propagate through the TGO into the bond coat asperities and then propagate in the ceramic again (Fig. 7b). The corresponding impressions of such regions can also be found in the ceramic top coat (Fig. 7b) showing the remnant TGO at the bond coat asperities. It was also seen that in all of these exceptional cases, there is a region brighter than the TGO but darker than the bond coat, indicating the presence of oxides of heavier elements of the bond coat. There are no such regions in the initial bond coat cross-section, they develop only later during the cyclic life. Further study of these regions using elemental mapping revealed that these regions are primarily oxides of chromium (Fig. 8). These heavier oxides are closer to the TGO–bond coat interface in the bond coat. The presence of chromia well within the bond coat is rare and occurs only around porosities in the bond coat. The origin and propagation of cracking in the ceramic top coat was similar for the three temperatures.

3.3. Oxide thickness

TGO thickness measured at various fractions of the total spallation life for the three temperatures, when plotted against the square root of the number of 1-h cycles, results in an almost linear trend (Fig. 9). This indicates that the oxide growth follows the parabolic rate law typical of continuous scales, given by:

$$h^2 = k_p t \quad (2)$$

where h is the thickness, t is the time and k_p is the parabolic rate constant. The slope of the linear trend lines in Fig. 9 is proportional to the square root of the parabolic rate constant at the specified temperature. The values thus obtained for the parabolic rate constants from the experimental results are 1.6×10^{-17} m^2/s at 1100 °C, 2.5×10^{-17} m^2/s at 1121 °C and 6.4×10^{-17} m^2/s at 1151 °C. These values agree very well with parabolic rate constants for alumina formers in literature [5,11,13]. Due to the presence of TGO (≈0.7 μm thick) in the as-received samples (prior to thermal cycling), the experimental results do not strictly follow Eq. (1), and the curves in Fig. 9 do not intersect the origin. However, the parabolic rate constant values are obtained from the slope of the lines, and the presence of initial TGO does not result in large errors. The study of three different temperatures also enables us to comment on the activation energy of α-alumina

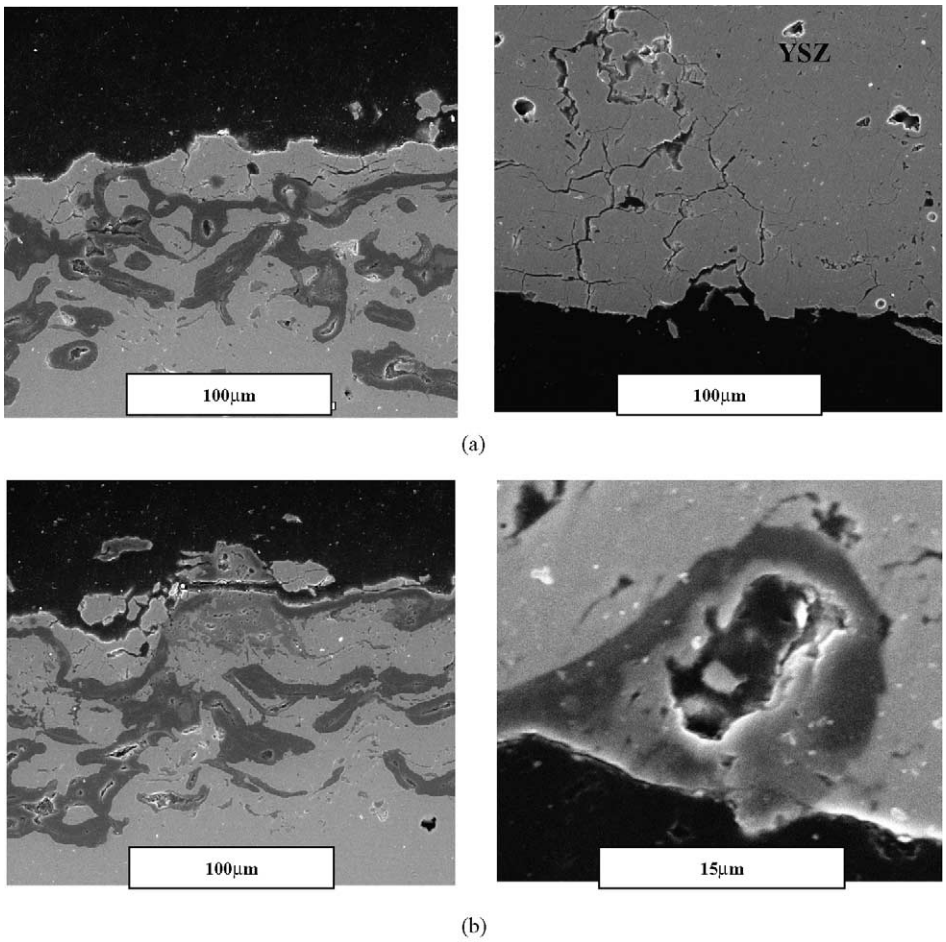

Fig. 7. Failed cross-sections of the TBC: (a) substrate and corresponding ceramic top coat entire crack growth is in ceramic; (b) substrate and corresponding ceramic top coat with cracking through the bond coat.

growth. The parabolic rate constant can be approximated to have the temperature dependence given by the Arrhenius equation.

$$k_p = A\exp^{(-E_a/RT)} \quad (3)$$

From the curves for the oxide growth at the three temperatures (Fig. 10), we can confirm that these relationships are closely followed in the oxidation behavior. The slopes of the trend lines are proportional to the square roots of the parabolic rate constants at a particular temperature, the increasing slopes with temperature in the experimental results conform to the trend expected based on Eq. (3). A plot of natural log of parabolic rate constant against reciprocal of the absolute temperature is shown in Fig. 10. The activation energy for α-alumina growth obtained from Fig. 10 was found to be 446 kJ/mole. Experimentally calculated values for activation energy of oxygen grain boundary diffusion in polycrystalline alumina are 460 ± 60 kJ/mole [14,15], the value of activation energy obtained here is consistent with grain boundary diffusion as the rate-controlling step in TGO growth. Oxide thickness at failure at all the temperatures lies within a very narrow range of 5–6 μm, indicating that mechanisms pertaining to critical thickness may have a role to play in these TBCs [10,14].

3.4. Bond coat rumpling

Image analysis was used to calculate the average roughness (R_a) of the ceramic–bond coat interface. A sampling length of 15 mm was used for each sample. The extent of rumpling was fairly extensive on the unconstrained bottom surface of the bond coat (Fig. 11), indicating that this particular NiCrAlY bond coat had a tendency to rumple with thermal cycling. However, mechanical constraint of TBC, especially for the dense low-stress TBC as in the present case, will reduce the rumpling rate. Average roughness (R_a) of the bond coat to ceramic top coat interface increased from 17 μm in the as-received condition to 24 μm at 80% of the life fraction for 1121 °C (Fig. 12). The average roughness at 80% life fraction for the samples tested at 1100 °C also increased from 17 μm to 25 μm. The DVC TBC specimen tested at 1151 °C at 75% of its life fraction showed an increased roughness to ≈27 μm. The average roughness values close to failure in the DVC TBC specimen for all three

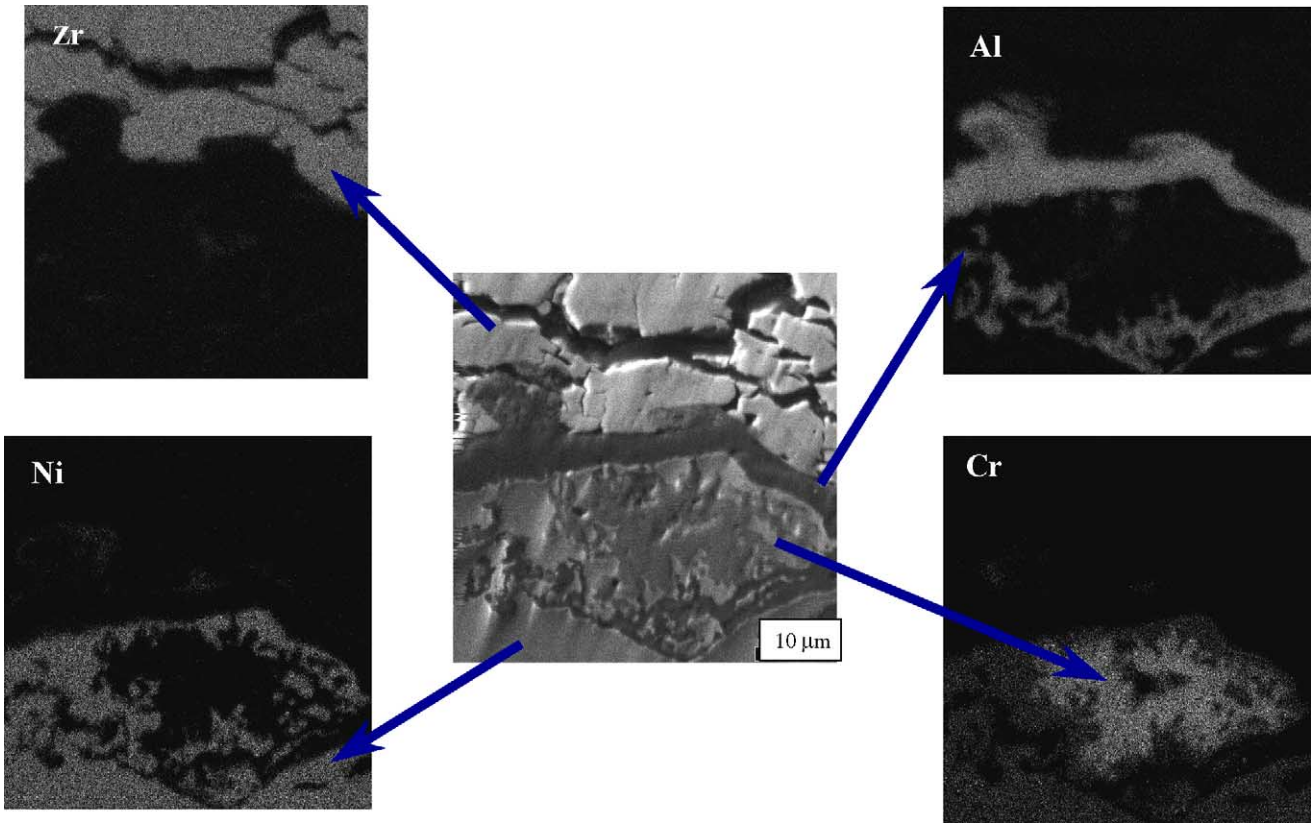

Fig. 8. Elemental maps using EDAX showing the presence of chromium oxides within the bond coat.

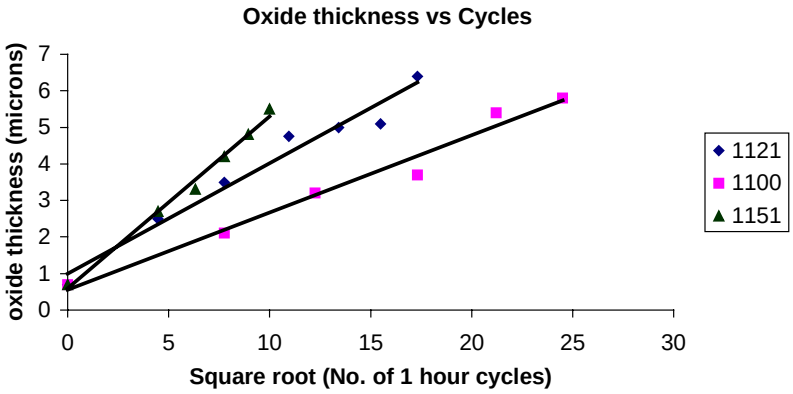

Fig. 9. Oxide thickness (μm) plotted against square root of number of cycles for three different temperatures.

temperatures lie within a relatively narrow range of 24–27 μm.

4. Discussion

Failure lives were determined for the DVC TBC specimens at 1100 °C, 1121 °C and 1151 °C. The variation in failure lives for a particular temperature was not large and the samples showed consistent results for each temperature tested. However, the failure lives showed a significant dependence on cycling temperature. The mechanism and mode of failure at the three temperatures was same. Failure occurred entirely in the ceramic parallel to the TBC–TGO interface and within ≈50 μm of the interface. This very strong and consistent dependence of failure lives on the cycling temperature can be explained by the effect of temperature on the extent of oxidation and roughening of the bond coat with thermal cycling.

Roughening or rumpling of the bond coat is an important issue in determining the failure life and mechanism of a TBC system [15–20]. If the interfaces were absolutely flat and no critically-sized flaws existed, then there would be no large contiguous areas of out-of-plane tensile stress known

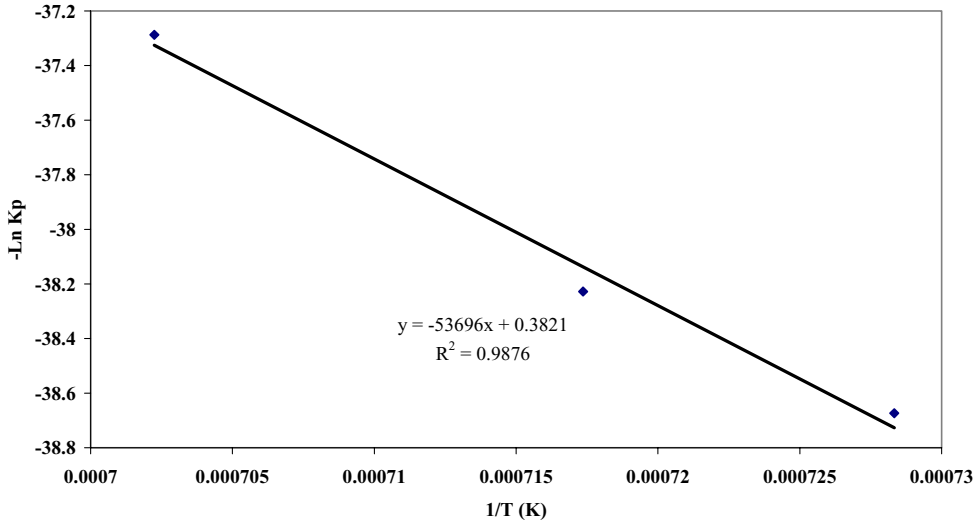

Fig. 10. Negative of the natural log of parabolic rate constants at three different temperatures vs. $1/T$ (K).

to cause failure in TBCs [16]. Rumpling has been extensively studied and modeled [21–28], and in many cases it has been attributed to cyclic plasticity. In a dissenting view, it has been attributed to stress driven surface diffusion [22]. In the case of cyclic plasticity driven rumpling, a critical role is played by the in-plane growth of the oxide [21,24–28]. In mechanisms based on cyclic plasticity, rumpling is accelerated if the initial surface is rough, which is true of the current case. Experiments have shown that isothermal exposure [23] and cycling with initially smooth surfaces [29] do not produce rumpling, while other conflicting experiments show that for different bond coat compositions, smooth samples under isothermal exposure do rumple [22]. The meaning of these contradictory results and a decisive explanation of the cause of rumpling in a given case is yet to be resolved, and this issue is beyond the scope of the present paper.

The proposed explanation for the observed failure, which occurs strictly in the ceramic layer and shows strong temperature dependence, is as follows:

1. Geometry changes imposed on the ceramic by changes in bond coat interface geometry cause stresses in the ceramic layer that cause cracking in the ceramic leading to failure.
2. The geometry changes are a result of both the effects of non-volume conserving oxidation [30] and progressive rumpling.

The proposed explanation is consistent with the four observations of the present study. First, the severity of rumpling at failure was approximately constant across specimens tested at different temperatures, with the average bond coat roughness (R_a) increasing from an initial value of $\approx$17 μm to $\approx$25 μm at failure. Thus, life reduction with increased temperature was produced by the increased rumpling rate with temperature. Second, the cracking was progressive and (Fig. 6) paralleled the development of bond coat roughness, due to rumpling, with thermal cycling (Fig. 12). Third, the failure was exclusively within the ceramic (Figs. 5 and 7). Fourth, the most common alternate failure mechanism, in which the strain energy in the thermally grown oxide generates failure often initiating at bond coat asperities, did not occur. In the DVC TBCs tested, the crack nucleation and propagation occurred in the ceramic, away from the ceramic–TGO interface, thus the high strain energy in the oxide plays no role in the spallation. For this proposed mechanism, suppression of rumpling would increase coating spallation life. Attempts to reduce rumpling in MCrAlY bond coats have been made in the past in order to increase the coating life by changing the bond coat chemistry [31] and the initial bond coat roughness [23].

The acceleration of rumpling with increased temperature can be explained in part by the reduction in strength of the bond coat with temperature [32] making it more susceptible to rumpling and in part by the increase in oxidation rate where the in-plane growth of the oxide has been shown by modeling [21,23–28] to be essential to the rumpling process. It is reasonable to expect that in-plane oxide growth occurs concurrently with increases in oxide thickness, and as a result, the higher oxide growth rates at higher temperatures leads to faster rumpling. The 4× reduction of life with increased temperature is consistent with the roughly 4× shorter time needed to grow the oxide to a critical thickness of about 6 μ and to achieve a surface roughness of 24–27 μm by rumpling. TGO growth drives both the geometry change associated with non-volume conserving oxidation and rumpling, both leading to TBC cracking in the present case.

Finally, internal oxidation of the bond coat plays only a minor role in the failure of DVC TBC coatings as it occupies less than 5% of the fracture area. The presence of interconnected porosity in the bond coat leads to faster depletion of Al in the bond coat. When the Al content is not sufficient to make a continuous Al_2O_3 scale, oxides of heavier elements

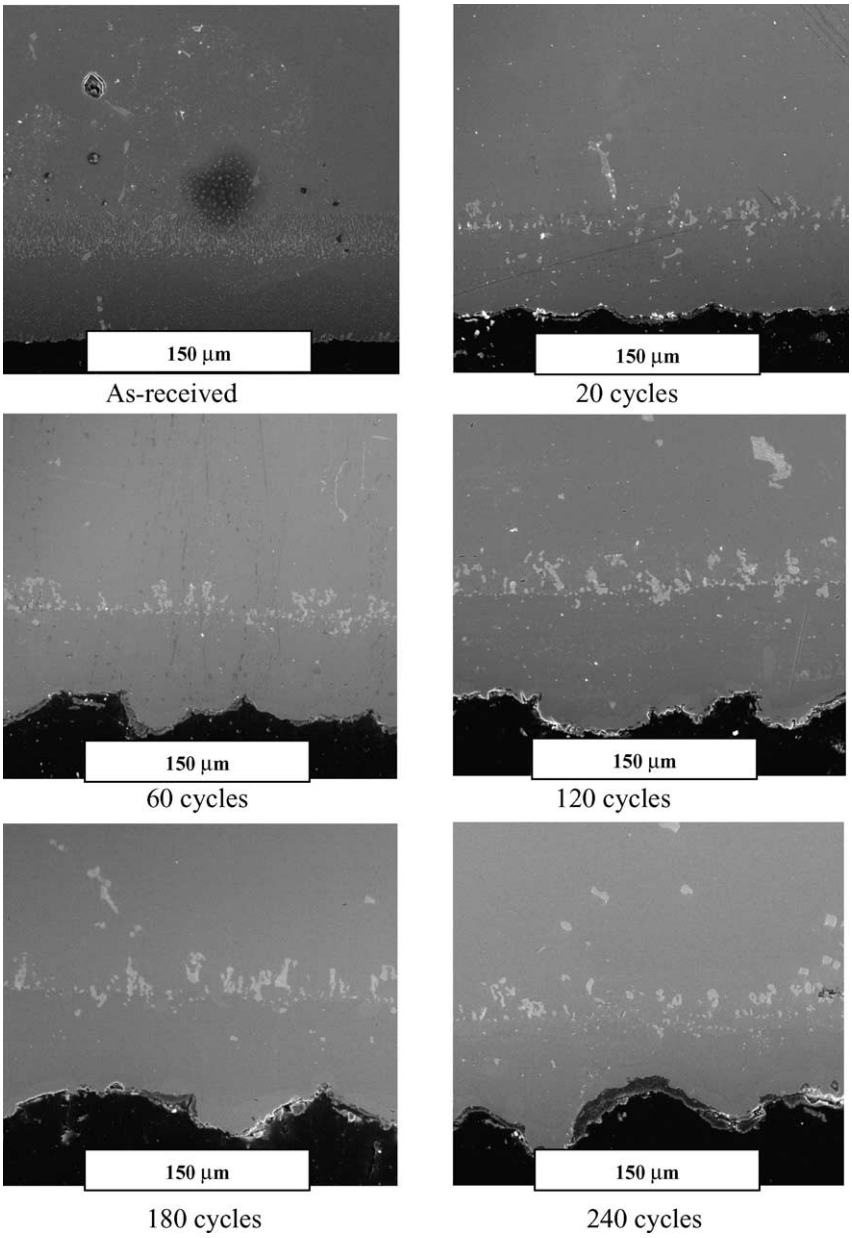

Fig. 11. Cross-section SEM micrographs of the bare bond coated side showing progressive distortion of the bond coat with thermal cycling.

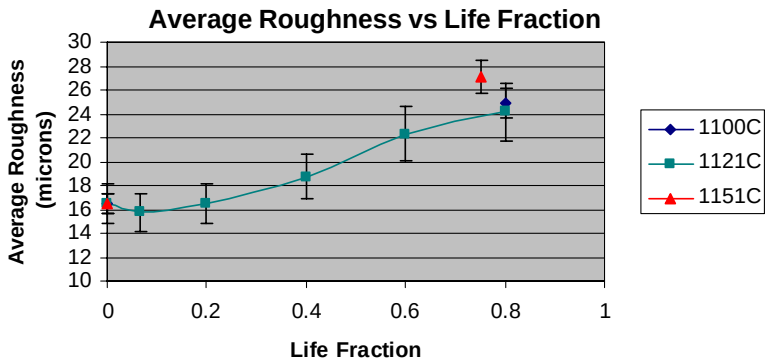

Fig. 12. Average roughness (R_a) vs. life fraction of the bond coat for the TBC coated side at 1100 °C, 1121 °C and 1151 °C.

in the bond coat form. The rate of Al depletion is higher at higher temperatures due to higher reaction rates. Chromia, confirmed by EDAX, appears only in the late stages of thermal cycling, when the aluminum content of the bond coat is severely depleted.

5. Conclusions

Failure mechanism for the dense vertically-cracked TBC investigated was determined at 1100 °C, 1121 °C and 1151 °C. The following conclusions can be made based on results obtained and discussed.

1. Thermal cycling temperature has a strong effect on failure lives for the DVC TBCs. An increase in cycling temperature from 1100 °C to 1151 °C resulted in a 6× decrease in failure life.
2. The failure mechanism observed for DVC TBC coatings was the same at the three temperatures.
3. Progressive TBC cracking was observed, beginning about 25% of the expected life, in the TBC parallel to the TBC–TGO interface and within 50 μm of the interface.
4. Crack density increased approximately linearly with cycles.
5. The roughness of the bond coat on both the TBC coated side and bare bond coat side increases with thermal cycling. The evidence presented then is consistent with the notion that cracking is caused by stresses imposed on the TBC due to shape changes in the bond coat.
6. Bond coat rumpling is faster at higher temperatures, thus reaching a critical range (24–27 μm) with fewer cycles.
7. TGO growth rates were parabolic and grain boundary diffusion of oxygen was the rate-determining step for the oxidation.
8. Reaction rate constants were higher at higher temperatures; thereby, promoting higher TGO growth rates and Al depletion from the bond coat.
9. TGO thickness was between 5 μm and 6 μm at failure at all three temperatures, indicating critical TGO thickness mechanisms may be active.
10. Secondary role in the failure of DVC TBC system was played by formation of chromia as aluminum depleted from the bond coat. The role of chromia in failure is indicated by fracture path going through chromium oxide layers.

Acknowledgements

This research was funded by Department of Energy under the Advanced Gas Turbine System Research (AGTSR) Program (Contract # 02-01-RR97), administered by the South Carolina Institute for Energy Studies, Clemson University.

References

[1] N.P. Padture, M. Gell, E.H. Jordan, Science 296 (2002) 280.
[2] R.A. Miller, J. Am. Ceram. Soc. 67 (1984) 517.
[3] R.L. Jones, in: K.H. Stern (Ed.), Metallurgical and Ceramic Protective Coatings, Chapman and Hall, London, 1996, p. 195.
[4] J.T. DeMasi-Marcin, D.K. Gupta, Surf. Coat. Technol. 68–69 (1994) 1–9.
[5] A.G. Evans, D.R. Mumm, J.W. Hutchinson, G.H. Meier, F.S. Pettit, Prog. Mater. Sci. 46 (2001) 505.
[6] E.Y. Lee, R.R. Biederman, R.D. Sisson, Mater. Sci. Tech. A121 (1989) 467.
[7] B.C. Wu, E. Chang, S.F. Chang, C.H. Chao, Thin Solid Films 172 (1989).
[8] R.A. Miller, C.E. Lowell, Thin Solid Films 95 (1982) 280.
[9] T.A. Taylor, US Patent No. 5,073,433 (1991).
[10] A. Rabei, A.G. Evans, Acta Mater. 48 (2000) 3963–3976.
[11] H.E. Eaton, J.R. Linsey, R.B. Dinwiddie, in: T.W. Tong (Ed.), Thermal Conductivity 22, Technomic, Lancaster, PA, 1994, p. 289.
[12] B. Zhou, K. Kokini, Mater. Sci. Eng. A348 (2003) 271.
[13] U. Schulz, M. Menzebach, C. Leyens, Y.Q. Yang, Surf. Coat. Technol. 146–147 (2001) 117–123.
[14] E. Dorre, H. Hubner, Alumina Processing, Properties and Application, Springer-Verlag, New York, 1984.
[15] M.W. Brumm, H.J. Grabke, Corros. Sci. Eng. 33 (11) (1992) 1677–1690.
[16] K.W. Schlichting, N.P. Padture, E.H. Jordan, M. Gell, Mater. Sci. Eng. A342 (2003) 120–130.
[17] P. Deb, D.H. Boone, T.F. Manley, J. Vacuum Sci. Technol. A5 (1987) 1209.
[18] J.W. Holmes, F.A. McClintock, Metall. Mater. Trans. 21A (1990) 1209.
[19] Y.H. Zhang, P.J. Withers, M.D. Fox, D.M. Knowles, Mater. Sci. Tech. 15 (1999) 1031.
[20] V.K. Tolpygo, D.R. Clarke, Acta Mater. 51 (2000) 239–249.
[21] Z. Suo, J. Phys. Mech. Solids 43 (1995) 829–846.
[22] R. Panat, S. Zhang, K.J. Hsia, Acta Mater. 51 (2003) 239–249.
[23] M. Gell, K. Vaidyanathan, B. Barber, J. Cheng, E. Jordan, Metall. Mater. Trans. 30A (1999) 427–435.
[24] A.M. Karlsson, J.W. Hutchinson, A.G. Evans, Mater. Sci. Eng. A351 (2003) 244–257.
[25] A.M. Karlsson, J.W. Hutchinson, A.G. Evans, J. Mech. Phys. Solids 50 (2002) 1565–1589.
[26] A.M. Karlsson, A.G. Evans, Acta Mater. 49 (2001) 1793.
[27] A.M. Karlsson, C.G. Levi, A.G. Evans, Acta Mater. 50 (2002) 1263.
[28] J.M. Ambrico, M.R. Begley, E.H. Jordan, Acta Mater. 49 (2001) 1577–1588.
[29] K. Vaidyanathan, M. Gell, E.H. Jordan, Surf. Coat. Technol. 133–134 (2000) 28–34.
[30] A.M. Freborg, B.L. Ferguson, W.J. Brindley, G.J. Petrus, Mater. Sci. Eng. A245 (1998) 182–190.
[31] R.C. Pennefather, D.H. Boone, Surf. Coat. Technol. 76–77 (1995) 47–52.
[32] D. Pan, M.W. Chen, P.K. Wright, K.J. Hemker, Acta Mater. 51–58 (2003) 2205.